Geophysical Journal International

Geophys. J. Int. (2017) **211,** 1328–1340
Advance Access publication 2017 August 4
GJI Seismology

doi: 10.1093/gji/ggx333

Crustal structure of the Transantarctic Mountains, Ellsworth Mountains and Marie Byrd Land, Antarctica: constraints on shear wave velocities, Poisson's ratios and Moho depths

C. Ramirez,[1] A. Nyblade,[1] E.L. Emry,[2] J. Julià,[3] X. Sun,[4] S. Anandakrishnan,[1] D.A. Wiens,[5] R.C. Aster,[6] A.D. Huerta,[7] P. Winberry[7] and T. Wilson[8]

[1]*Department of Geosciences, The Pennsylvania State University, University Park, PA* 16802, *USA. E-mail: crsito_15@yahoo.com*
[2]*Earth and Environmental Sciences, New Mexico Institute of Mining and Technology, Socorro, NM* 87801, *USA*
[3]*Departamento de Geofisica & Programa de Pós-Graduação em Geodinâmicae Geofísica, Universide Federal do Rio Grando do Norte, Natal, Rio Grande do Norte, Brazil*
[4]*Guangzhou Institute of Geochemistry, Chinese Academy of Sciences, GD* 510640 *Guangzhou, China*
[5]*Department of Earth and Planetary Sciences, Washington University in St. Louis, St. Louis, MO* 63130, *USA*
[6]*Department of Geosciences, Warner College of Natural Resources, Colorado State University, Fort Collins, CO* 80523, *USA*
[7]*Department of Geological Sciences, Central Washington University, Ellensburg, WA* 98926, *USA*
[8]*School of Earth Sciences, The Ohio State University, Columbus, OH* 43210, *USA*

Accepted 2017 August 3. Received 2017 July 31; in original form 2016 November 23

SUMMARY

A uniform set of crustal parameters for seismic stations deployed on rock in West Antarctica and the Transantarctic Mountains (TAM) has been obtained to help elucidate similarities and differences in crustal structure within and between several tectonic blocks that make up these regions. *P*-wave receiver functions have been analysed using the H–κ stacking method to develop estimates of thickness and bulk Poisson's ratio for the crust, and jointly inverted with surface wave dispersion measurements to obtain depth-dependent shear wave velocity models for the crust and uppermost mantle. The results from 33 stations are reported, including three stations for which no previous results were available. The average crustal thickness is 30 ± 5 km along the TAM front, and 38 ± 2 km in the interior of the mountain range. The average Poisson's ratios for these two regions are 0.25 ± 0.03 and 0.26 ± 0.02, respectively, and they have similar average crustal Vs of 3.7 ± 0.1 km s^{-1}. At multiple stations within the TAM, we observe evidence for mafic layering within or at the base of the crust, which may have resulted from the Ferrar magmatic event. The Ellsworth Mountains have an average crustal thickness of 37 ± 2 km, a Poisson's ratio of 0.27, and average crustal Vs of 3.7 ± 0.1 km s^{-1}, similar to the TAM. This similarity is consistent with interpretations of the Ellsworth Mountains as a tectonically rotated TAM block. The Ross Island region has an average Moho depth of 25 ± 1 km, an average crustal Vs of 3.6 ± 0.1 km s^{-1} and Poisson's ratio of 0.30, consistent with the mafic Cenozoic volcanism found there and its proximity to the Terror Rift. Marie Byrd Land has an average crustal thickness of 30 ± 2 km, Poisson's ratio of 0.25 ± 0.04 and crustal Vs of 3.7 ± 0.1 km s^{-1}. One station (SILY) in Marie Byrd Land is near an area of recent volcanism and deep (25–40 km) seismicity, and has a high Poisson's ratio, consistent with the presence of partial melt in the crust.

Key words: Structure of the Earth; Antarctica; Crustal structure.

1 INTRODUCTION

Over the past two decades there has been a historic increase in broadband seismic networks deployed in Antarctica for investigating deep Earth structure beneath major tectonic features, such as the Transantarctic Mountains (TAM), the Gamburtsev Subglacial Mountains, the West Antarctic Rift System (WARS), and Marie Byrd Land (MBL). Seismic data recorded by these networks have been analysed to obtain estimates of crustal structure, such as Moho depth and Poisson's ratio, leading to an improved understanding of Antarctica's crust. However, data from the different networks have been analysed separately with a variety of methods, yielding information on crustal properties that varies among studies. For example, Finotello *et al.* (2011) reported estimates of Moho depth and mean

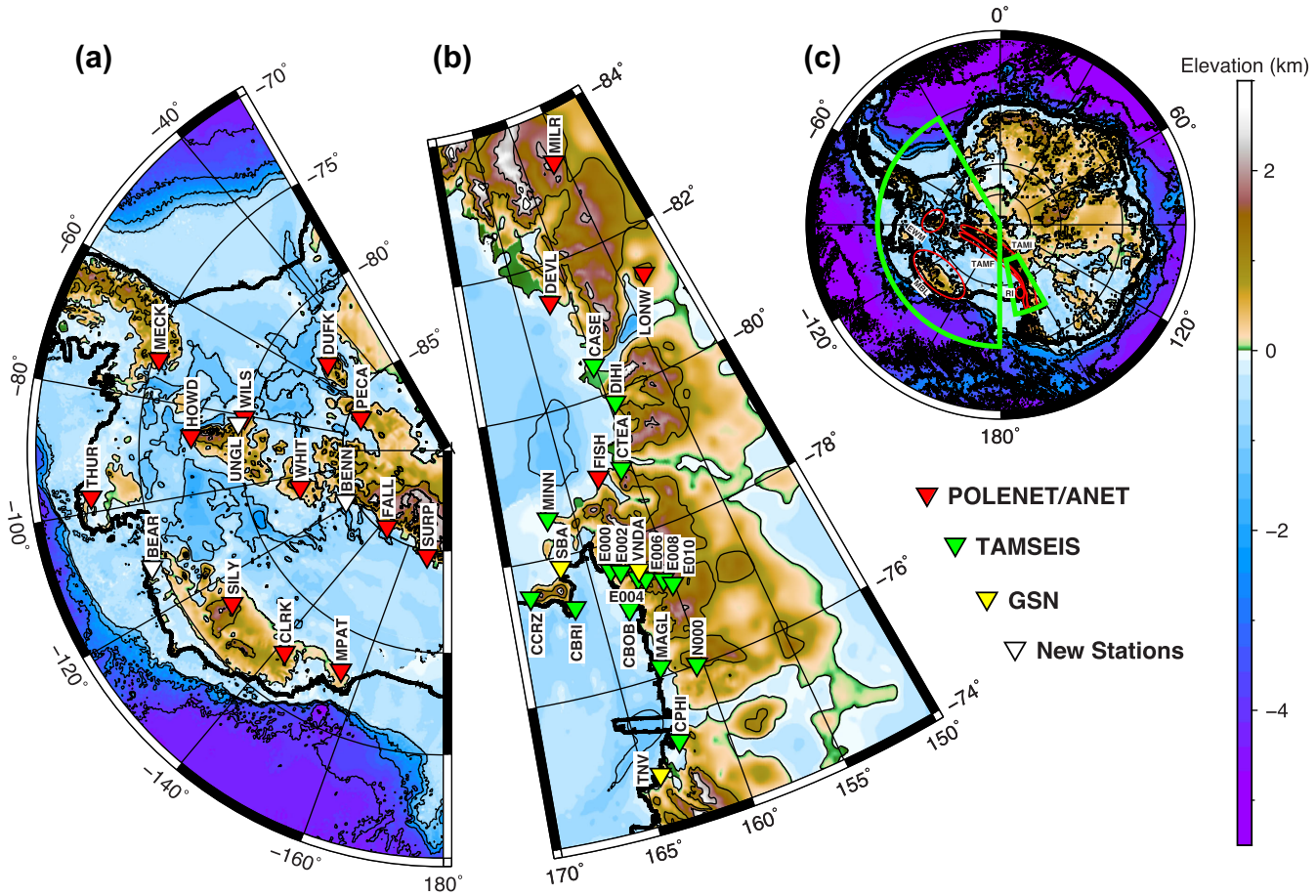

Figure 1. Seismic stations used in this study plotted on maps showing bed elevations (Fretwell *et al.* 2013). (a) Locations of POLENET/ANET seismic stations (triangles) used in West Antarctica. The white triangles indicate location of stations from which no previous results are available. (b) Location of TAMSEIS (green triangles), POLENET/ANET (red triangles) and Global Seismic Networks (yellow triangles) stations on Ross Island and a portion of the TAM. (c) Map of Antarctica outlining the regions in (a) and (b) in green, as well as the tectonic regions mentioned in the text outlined in red.

crustal Vp/Vs for one set of stations in the TAM and on Ross Island, but no information on crustal *P*- or *S*-wave velocities. In contrast, Chaput *et al.* (2014) reported estimates of Moho depth and crustal *P*-wave velocities for rock and ice sites within the TAM and West Antarctica (WA), but for models with constrained Vp/Vs. Obtaining a uniform set of crustal parameters for Antarctica is also challenging because *P*-wave receiver functions from seismic stations deployed on ice sheets are complicated by reverberations within the ice layer, which can lead to lower resolution crustal structure models (Hansen *et al.* 2010; Chaput *et al.* 2014; Graw *et al.* 2016). To compile a uniform set of crustal parameters for stations deployed on ice, Ramirez *et al.* (2016) applied a standard modelling approach using *S*-wave receiver functions and Rayleigh wave phase velocities for broadband stations in WA, the TAM, as well as a number stations in East Antarctica (EA).

In this companion paper, we provide a uniform set of crustal parameters, including Moho depth, a crustal shear wave velocity profile, and crustal Poisson's ratio, for broadband stations in WA and TAM deployed on rock by analysing *P*-wave receiver functions and Rayleigh wave phase and group velocities using the H–κ stacking method of Zhu & Kanamori (2000) and the joint inversion approach of Julià *et al.* (2000). The seismic stations are part of the 2000–2003 TAMSEIS (Lawrence *et al.* 2006a) and 2009–2015 POLENET/A-NET (Lloyd *et al.* 2015) experiments. No previous estimates of crustal structure have been reported before for three of the POLENET/ANET stations, and results obtained for several stations are different from crustal structure reported in previous studies. Our findings thus expand upon existing constraints on crustal thickness and composition, enabling us to examine more comprehensively than before the nature of the crust beneath several tectonic blocks making up WA and the TAM, and to comment further on their origin.

2 TECTONIC BACKGROUND

In this section, we describe the tectonic history of several blocks within WA and the TAM for which we provide new information on crustal structure (Fig. 1).

2.1 Transantarctic Mountains

The TAM are a geologic and topographic boundary dividing stable EA from a more tectonically active WA (Fig. 1). The TAM span roughly 3500 km in length and reach elevations as high as 4500 m (ten Brink *et al.* 1997). The basement rocks of the TAM are composed of Precambrian/Cambrian metasediments combined with Ordovician granites and Devonian intrusives. During the Devonian to the Triassic, the Beacon Supergroup formed, and in the Cenozoic, volcanism was followed by marine, lacustrine and glacial

sedimentation in some locations, capping off the TAM (Fitzgerald 1992). Because areas along the coast have been affected by the tectonics of the WARS, we group stations located along the Transantarctic Mountains front (TAMF) separately from stations in the interior of the Transantarctic Mountains (TAMI).

2.2 Ellsworth Mountains

The Ellsworth Mountains (EWM) are a mountain range about 350 km long and about 80 km wide (Webers *et al.* 1992) separating the interior of WA from the Antarctic Peninsula and the Weddell Sea. The EWM are composed mostly of clastic sedimentary rocks with minor portions of igneous intrusions and volcanics, as well as some limestones (Yoshida 1982). Timing of the uplift and major deformation events of the EWM, including the translation/rotation from the TAM to their present location, is not well constrained, but most likely occurred during the Jurassic and Cretaceous (Webers *et al.* 1992; Dalziel *et al.* 2013).

2.3 Marie Byrd Land

MBL covers an area of roughly 1000 km × 500 km in the northern section of WA between the Amundsen Sea and the Ross Sea. The area is characterized by Late Cenozoic alkalic volcanism (LeMasurier & Rex 1989), and many studies link the uplift of MBL to a mantle plume. LeMasurier & Rex (1989) suggested the presence of a mantle plume based on the timing and alignment of the volcanic chains within MBL. Seismic studies also provide some evidence for a mantle plume. Lloyd *et al.* (2015) and Heeszel *et al.* (2016) imaged a prominent low velocity zone extending to at least 200 km depth beneath MBL. Using migrated stacks of receiver functions, Emry *et al.* (2015) imaged mantle transition zone thinning in adjacent areas to MBL beneath the Bentley Subglacial Trench and Ruppert Coast, and Accardo *et al.* (2014) found a shear wave splitting pattern across MBL consistent with mantle flow from a plume. Hansen *et al.* (2014), imaging deeper into the mantle than Lloyd *et al.* (2015) and Heeszel *et al.* (2016), suggested that the low velocity anomaly beneath MBL may extend through the mantle transition zone and into the lower mantle.

2.4 Ross Island

Ross Island (RI) is part of a Cenozoic volcanic province that lies at the eastern end of the Terror rift (Trey *et al.* 1999) and includes Mt. Erebus (Hall *et al.* 2007), which is an active volcano. Kyle (1990) suggested that a mantle upwelling or a hotspot is present beneath RI based on the large volume of phonolite lavas erupted and doming of the area. Lawrence *et al.* (2006b) and Watson *et al.* (2006) found seismic evidence for a thermal anomaly in the upper mantle beneath RI, consistent with a plume interpretation for the hotspot, and Hansen *et al.* (2014) showed that the low seismic velocity anomaly imaged is predominantly restricted to the upper 200–300 km of the mantle.

2.5 Previous crustal results from passive source seismic studies

A number of previous studies have reported information on crustal structure in the TAM and WA using data from stations that we also used in this study. Lawrence *et al.* (2006c) utilized a genetic algorithm to search crustal thickness and velocity space to obtain models that fit receiver functions for the TAMSEIS stations. They found the TAM coastal area to have crust over 20 km thick, and in the interior of the TAM crust that is ∼40 km thick (Lawrence *et al.* 2006c).

Finotello *et al.* (2011) conducted a study using the H–κ stacking method for the TAMSEIS rock stations, finding crustal thicknesses of 19–39 km and Vp/Vs values ranging from 1.63 to 1.78, indicating a felsic to intermediate composition for the crust. They also obtained a Vp/Vs of 1.88 within the RI area, which they attributed to mafic crust, consistent with the composition of volcanic rocks from Mt. Erebus.

Chaput *et al.* (2014) investigated crustal structure beneath POLENET/ANET stations by using a Markov Chain Monte Carlo inversion scheme to model *P*-wave receiver functions that could accommodate reverberations from thick ice sheets. They reported crustal thicknesses for MBL, TAM and EWM of roughly 30 km, and also showed that each of these regions is separated by thinner (20–25 km) crust beneath the WARS.

Estimates of crustal structure in the TAM have also been reported by Pondrelli *et al.* (1997) and Bannister *et al.* (2003) using receiver function from data recorded on other temporary seismic stations. Pondrelli *et al.* (1997) used receiver functions from a temporary array of seismic stations near RI. They found that the crust near the coast is 25 km thick and thickens to ∼43 km over a horizontal distance of ∼100 km in the central section of the mountain range. Similarly, Bannister *et al.* (2003) modelled data from seismic stations in the TAM near RI to image crustal structure. Consistent with other studies, they found that the coastal region is dominated by ∼18–20 km thick crust that rapidly increases to ∼35–40 km in the interior of the TAM.

3 DATA AND METHODS

3.1 Data

The data used in this study to compute receiver functions come from two different temporary seismic networks, the 2000–2003 TAMSEIS network (Lawrence *et al.* 2006a) and the 2009–2015 POLENET/A-NET network (Anthony *et al.* 2014; Lloyd *et al.* 2015; Fig. 1). In addition, we used data from three permanent stations, SBA, TNV and VNDA, which are located in the coastal area of the TAM near to or on RI (Fig. 1b). The TAMSEIS network was divided into three sub-arrays, a 16 station array with an east-west strike across the TAM, a 17 station N–S array extending from the TAM into the interior of EA, and a coastal array with 9 stations along the Antarctic coast near to and within RI (Lawrence *et al.* 2006b). Stations that were deployed on rock include all of the coastal array stations, several of the stations in the east-west array, and station N000 (Fig. 1). The POLENET/A-NET network consists of a backbone array of 24 stations and a temporary array of 13 stations deployed between 2010 and 2012 across the WARS. Fourteen of the backbone stations and two of the temporary stations were deployed on rock outcrops.

The joint inversion technique employed in this study, for all but one station, utilizes Rayleigh wave group velocity measurements from 8 to 60 s period and phase velocity measurements from 18 to 113 s period together with the receiver functions. The phase velocity measurements are taken from Heeszel *et al.* (2016) and group velocity measurements are from Sun *et al.* (2013). There were no group velocity measurements available for station THUR, and therefore only phase velocities were used in the inversion.

3.2 Receiver functions

Receiver functions are time series that encode the response of Earth structure beneath a recording station (Langston 1979) and are commonly used for investigating crustal structure. The main phases in the waveforms are the direct *P* wave, the *P*-to-*S* conversion at the Moho (Ps) and its reverberations between the Moho and the free surface (PpPs and PsPs + PpSs). The amplitudes and arrival times of these phases place valuable constraints on crustal structure beneath the receiver (Langston 1979) and are commonly used to estimate the thickness of the crust and the bulk crustal *P*-wave velocity/*S*-wave velocity (Vp/Vs) ratio (e.g. Zandt & Ammon 1995; Zhu & Kanamori 2000). *P*-wave receiver functions can also be jointly modelled with surface wave dispersion measurements to obtain a depth dependent profile of crustal *S*-wave velocities (Julía *et al.* 2000, 2003).

P-wave receiver functions were computed for each station using teleseismic events with magnitudes equal to or greater than 5.5 and located at epicentral distances between 30° and 90°. For calculating the *P*-wave receiver functions, the originally recorded seismograms were cut to 10 s before and 110 s after the first *P*-wave arrival. Then the waveforms were de-trended, tapered, high pass filtered above 0.05 Hz to remove low-frequency noise, and low pass filtered below 8 Hz. The data were then decimated to 10 samples s^{-1} and the horizontal components were rotated to the great circle path to obtain radial and transverse components. Finally, the vertical component was deconvolved from the radial and tangential components using 500 iterations in the iterative time-domain deconvolution method developed by Ligorría & Ammon (1999). For each teleseismic event, radial and tangential receiver functions were computed for Gaussian width factors of 1.0 ($f \leq 0.5$ Hz) and 2.5 ($f \leq 1.25$ Hz). Lower frequencies result in longer wavelength receiver functions, which are better for observing longer period phases from the lower crust and mantle, while higher frequency receiver functions can reveal detailed phases from shallow crustal structure (Owens & Zandt 1985; Ligorría & Ammon 1999).

The quality of the receiver functions was assessed using the L2-norm residual between the original radial component and the predicted radial component. The predicted radial component was generated by the convolution of the original vertical component and the radial receiver function. A residual of 15 per cent or less was used to select receiver functions for further analysis. In addition, receiver functions that showed unreasonably large amplitudes on both radial and transverse components were not considered for further processing, even if they passed the 15 per cent criterion. The same receiver functions from each individual station were used for both the *H*–κ stacking method and the joint inversion analysis.

3.3 H–κ stacking method

Crustal thickness estimated solely from the delay time between the Moho Ps phase and the direct *P*-wave trades off strongly with crustal Vp/Vs. Therefore, the H–κ stacking method of Zhu & Kanamori (2000) was applied to the receiver functions to obtain estimates for crustal thickness (H) and bulk Vp/Vs ratio (κ). The H–κ stacking method reduces the ambiguity in H and κ by incorporating the later multiple converted phases from the Moho (PpPs and PsPs + PpSs). The technique solves for the objective function *S* using eq. (1):

$$S(H_1, k_1) = w_1 r(t_1) + w_2 r(t_2) - w_3 r(t_3) \quad (1)$$

where t_i are the traveltimes of the three main *P*-to-*S* converted phases from the Moho (Ps, PpPs and PsPs + PpSs), w_i are weights assigned to each phase (sum of $w_i = 1$), and r_j is the receiver function amplitude for the *j*th receiver function. $S(H,\kappa)$ reaches its maximum when optimal values for *H* and κ are determined, satisfying a simple layer over a half-space crustal model.

To apply the *H*–κ stacking method to the receiver functions, weights for the converted phases (eq. 1) and an average crustal Vp must be selected. A weighting system of $w_1 = 0.7$, $w_2 = 0.2$ and $w_3 = 0.1$, was used, similar to Zhu & Kanamori (2000). We chose a Vp of 6.5 km s^{-1} because this is a reasonable average value for continental crust (Christensen & Mooney 1995); however, we take into account uncertainties arising from this choice of Vp by computing *H*–κ stacks for a suite of *P*-wave velocities. The *H*–κ grid-search space spans 40 km, starting at depths that avoid inclusions of the direct *P*-wave arrival. Some of the stations displayed multiple maxima that required smaller windowing to isolate the most geologically plausible maxima. For these stations we provide results for both the wide parameter space grid-search and the narrowly focused one in the Supporting Information.

The *H*–κ stacking method was performed using both high- and low-frequency receiver functions for all stations. For seven of the stations (DEVL, FISH, MILR, UNGL, HOWD, MECK and THUR), the Moho Ps arrival and the crustal multiples were more pronounced on the higher frequency receiver functions and therefore results for these stations are reported from *H*–κ stacking of the high-frequency receiver functions. Formal uncertainties for *H* and κ were estimated using a bootstrapping method that repeats the summation procedure 200 times with random, resampled data from the original dataset with replacement (Efron & Tibshirani 1991). As previously mentioned, additional uncertainties in *H* and κ arise from the selection of mean crustal Vp, and therefore, the *H*–κ stacks were recomputed for *P*-wave velocities of 6.3 and 6.7 km s^{-1} to place lower and upper error bounds on *H* and κ for a range of crustal *P*-wave velocities. The reported uncertainties correspond to the addition of the bootstrap formal uncertainty and the range of values obtained using *P*-wave velocities of 6.3 and 6.7 km s^{-1}. An example for station WHIT is illustrated in Fig. 2 (see the Supporting Information for results from all stations).

Some of the stations are located on boundaries between tectonic blocks where abrupt changes in crustal thickness may occur. In such a situation, receiver functions from different backazimuths could be quite variable and simply stacking all of them to obtain a single model of crustal structure may not yield an accurate model. To check the receiver functions for indications of azimuthal variability, the Moho Ps conversion points beneath each station were mapped using a 30 km thick crust to determine the approximate locations of conversion points with respect to tectonic boundaries. The Moho Ps arrival times were then examined for variability between tectonic boundaries. No significant evidence was found for azimuthal variability at any of the stations.

3.4 Joint inversion of Rayleigh wave dispersion curves and receiver functions

To obtain crustal shear wave velocity models for each station, receiver functions were jointly inverted with Rayleigh wave phase and group velocities. While receiver functions mainly constrain shear wave velocity contrasts at interfaces between layers, Rayleigh wave dispersion curves place constraints on averages of the absolute shear wave velocity within frequency dependent depth ranges. Therefore, the combination of the two datasets provides tighter constraints on the shear wave velocity structure at depth and bridges the resolution

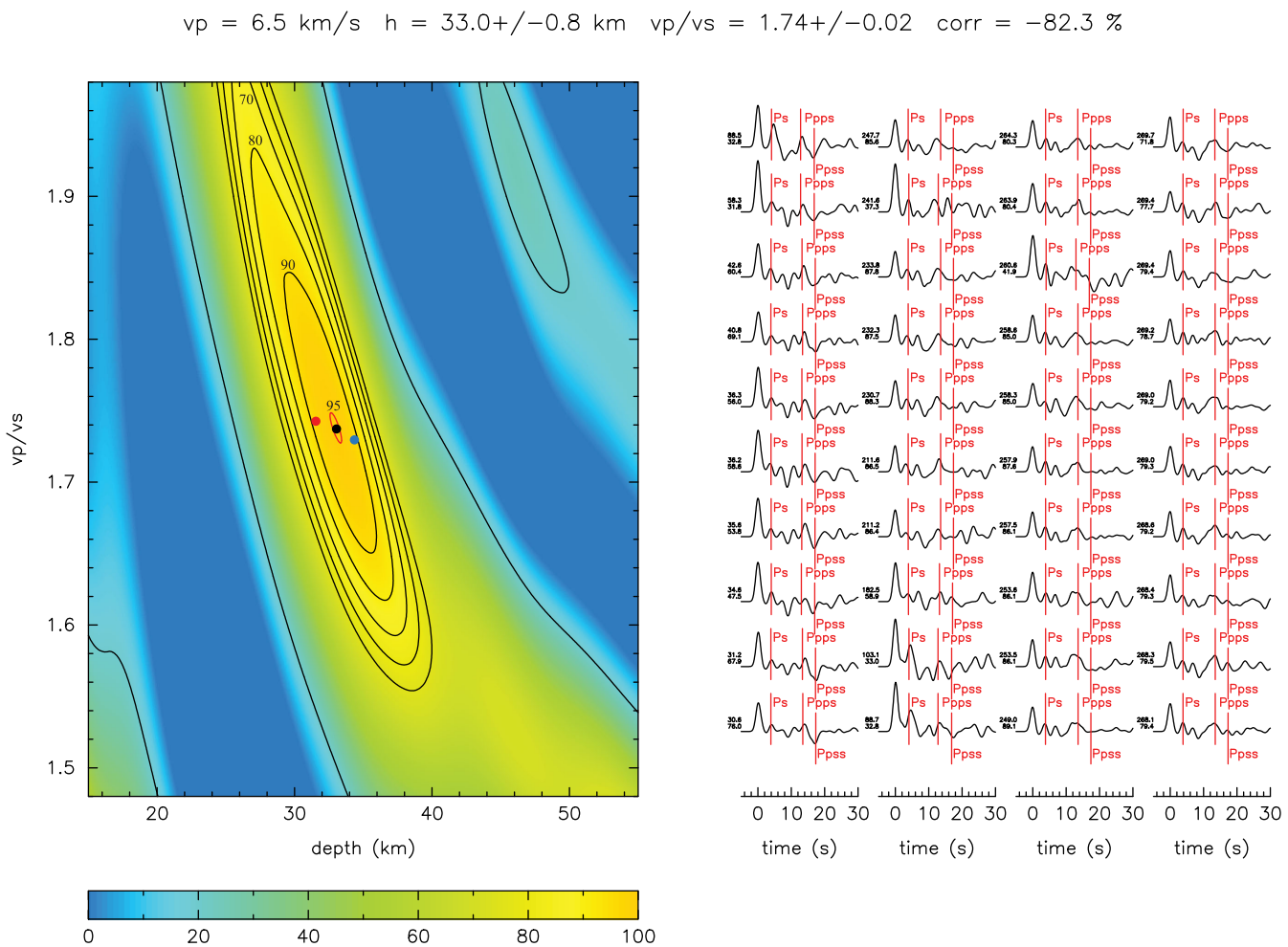

Figure 2. *H–κ* stack result for station WHIT. The parameter space of eq. (1) is shown on the left panel, where the center red circle indicates the 95 per cent confidence bound and the black contours indicate the fit to the objective function in 10 per cent increments. The red, black and blue dots show the *H* and *κ* values for the stacks using mean crustal Vp of 6.3, 6.5 and 6.7 km s^{-1}, respectively. The receiver functions are shown in black in the right panel with increasing backazimuth from bottom to top starting at the leftmost colum. The backazimuth and epicentral distance to the event are indicated in the top and bottom numbers to the left of each receiver function. The red lines indicate the theoretical arrival times of the labelled phases.

gaps inherent in each dataset individually. The inversion method used follows a linearized scheme that minimizes the least squares difference between observations and predictions and the roughness norm of the velocity-depth profile. The method also allows for *a priori* velocity constraints in select portions of the model (Julià *et al.* 2003).

Following Julia *et al.* (2000), the receiver function and surface wave dispersion datasets are equalized by the number of data points and physical units by dividing the RMS misfit for each data set by $N\sigma^2$, where 'N' is the number of data points and σ^2 is the variance. Since the receiver function data set may consist of several waveforms, the number of data points for the receiver function portion of the misfit function is the total number of points in the combined receiver function dataset. This makes the receiver function and surface wave dispersion datasets have equal weight in the misfit function, even when the number of receiver function waveforms is much larger than the number of dispersion curves.

Prior to performing the inversion, the dispersion measurements were smoothed using a three-point running average. Receiver functions were binned in ray parameter groups of 0.040–0.049, 0.050–0.059, 0.060–0.069, and greater than 0.070 s km^{-1} to account for phase-moveout from differing incident angles. The receiver functions were also stacked separately for two sets of overlapping frequency bands corresponding to Gaussian bandwidths of 1.0 ($f \leq 0.5$ Hz) and 2.5 ($f \leq 1.25$ Hz). Inverting receiver functions at several frequency bandwidths can help to distinguish sharp discontinuities from gradational ones in the velocity models (Cassidy 1992; Julià *et al.* 2005; Julià 2007).

The starting model used in the joint inversion is a 40-km-thick crust that has a linear shear wave velocity increase from 3.4 to 4.0 km s^{-1} and a Poisson's ratio determined from the *H–κ* stacking method. The crust lies over a flattened Preliminary Reference Earth Model (PREM) for the mantle (Dziewonski & Anderson 1981) down to 400 km depth. The mantle shear wave velocity structure is modelled to 290 km depth and then constrained to be equal to PREM below that depth. Layer thicknesses were fixed at 1 and 1.5 km for the top two layers of the model, 2.5 km between 2.5 and 65 km depth, 5 km between 65 and 190 km depth and 10 km below a depth of 265 km.

Uncertainties in the velocity models were estimated using the approach of Julià *et al.* (2005) by repeating inversions for a range of parameters, constraints and Poisson's ratios. This approach yielded uncertainties in the crustal shear wave velocity of individual layers of 0.1 km s^{-1} and 0.2 km s^{-1} in the upper mantle, which translate

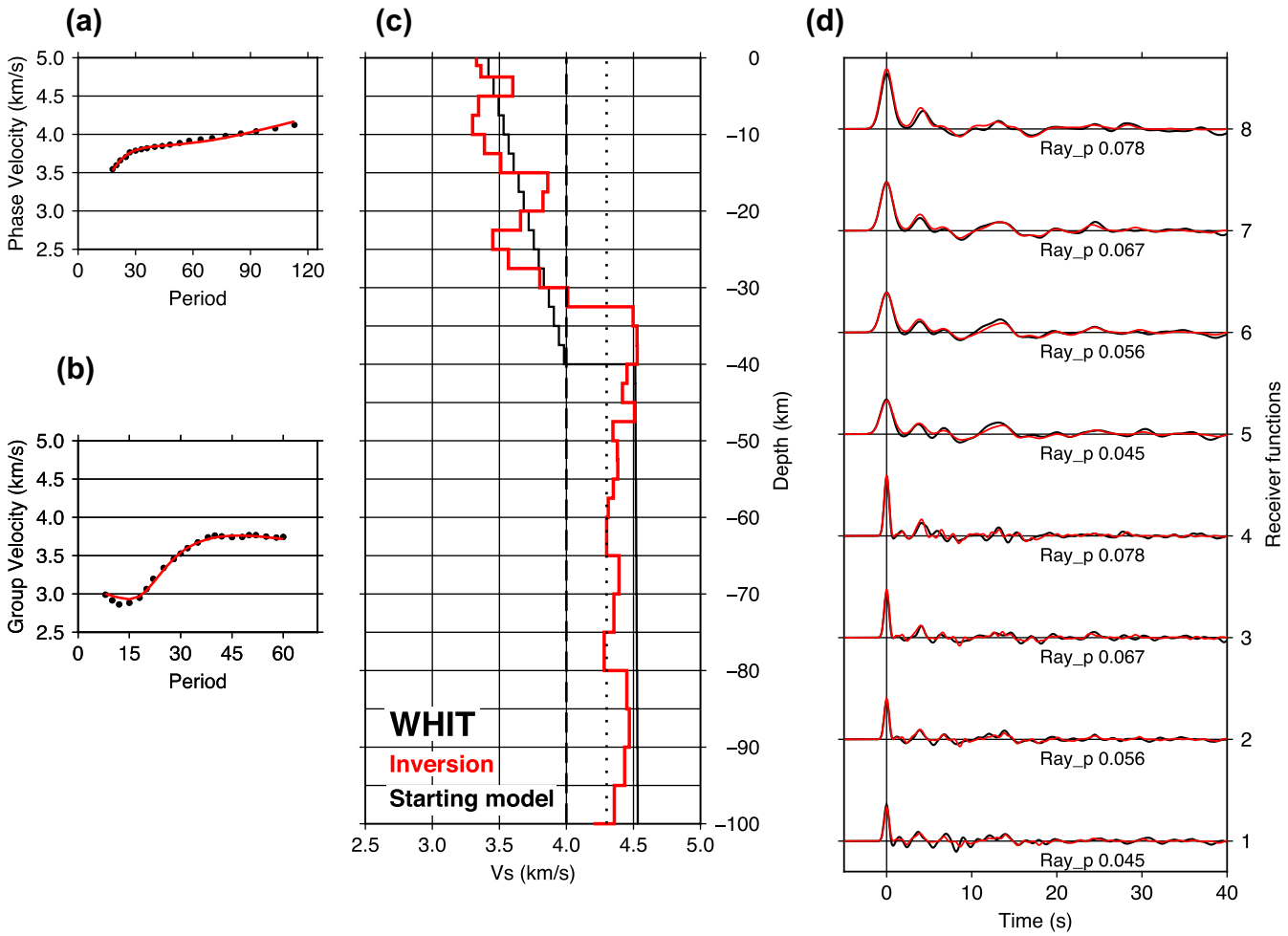

Figure 3. Joint inversion results for station WHIT. (a) The phase velocities obtained from Heeszel *et al.* (2016) are shown as the dotted black line and the solid red line shows the resulting phase velocity curve from the inversion. (b) The group velocities obtained from Sun *et al.* (2013) are shown as a dotted black line and the resulting group velocity curve from the inversion is shown as a solid red line. (c) Joint inversion velocity profile. The solid black line represents the initial model. The red line indicates the inversion result. The dashed line at 4.0 km s^{-1} and dotted line at 4.3 km s^{-1} are for reference. The Moho depth is selected where a large velocity discontinuity occurs (33 km). (d) Black lines are the receiver function stacks computed from the data and red line denotes the synthetic receiver function computed from the joint inversion result. The top four traces are the low-frequency receiver functions and the bottom four the high-frequency receiver functions. The ray parameter indicated is in the middle of the range used for each stack.

into uncertainties of ∼2.5 km in crustal thickness, roughly one layer thickness in the inversion scheme. The results for station WHIT are illustrated in Fig. 3 and the results for the other stations can be found in the Supporting Information, including plots of the receiver functions arranged by backazimuth, ray parameter and distance.

3.5 Selection criteria for Moho depths in 1-D velocity profile

While the H–κ stacking method yields a direct estimate of Moho depth, the shear wave velocity profile obtained from the joint inversion must be interpreted to obtain an estimate of crustal thickness. We chose the Moho in the joint inversion models to be the depth at which a significant increase in velocity occurs. For most of the stations, the shear wave velocity increases from $\leq$4.0 to $\geq$4.3 km s^{-1} at the depths selected as the Moho, consistent with a lithologic boundary between the crust and mantle. Shear wave velocities derived from experimentally determined Vp/Vs indicate that shear wave velocities in lower crustal rock assemblages tend not to exceed 4.3 km s^{-1} and those velocities of 4.3 km s^{-1} or higher are more common for mantle lithologies (Christensen & Mooney 1995; Christensen 1996).

We also obtain estimates of the thickness of a high velocity layer, interpreted as mafic material, in the lower crust from the joint inversion models. A number of previous studies of continental crustal structure (e.g. Holbrook *et al.* 1992; Christensen & Mooney 1995; Rudnick & Fountain 1995; Rudnick & Gao 2003) have reported that common lower crustal mafic lithologies, such as amphibolites, garnet-bearing and garnet-free mafic granulites and mafic gneisses, have higher shear wave velocities ($>$3.9 km s^{-1}) while intermediate-to-felsic lithologies have lower shear wave velocities ($<$3.9 km s^{-1}). Therefore, layers with shear wave velocities between 4.0 and 4.2 km s^{-1} immediately above the Moho can be interpreted as mafic lower crust.

4 RESULTS

The crustal thickness results from both the H–κ stacking and joint inversion methods are summarized in Table 1 and Fig. 4, along with results from previous studies. The Poisson's ratio estimates

Table 1. Summary of results.

Station	JI Moho depth (±3 km)	Average crustal Vs (±0.1 km s^{-1})	*H–κ* stacking Moho depth (km)	*H–κ* stacking crustal Vp/Vs	Poisson's ratio	Mafic lower crust (±3 km)	Chaput *et al.* (2014) Moho depth (km)
Transantarctic Mountains Front (TAMF)							
BENN	33	3.5	30 ± 2.7	1.87 ± 0.04	0.30 ± 0.01	0	—
CASE	30	3.7	24 ± 3.5[a]	1.73[a]	0.25	5	—
CBOB	23	3.7	30 ± 7.4[a]	1.73[a]	0.25	5	—
CTEA	30	3.7	30 ± 1.8[a]	1.78 ± 0.05[a]	0.27 ± 0.02	0	—
DIHI	30	3.7	33 ± 2.2[a]	1.63 ± 0.05[a]	0.20 ± 0.03	3	—
E000	23	3.7	25 ± 2.5[a]	1.73[a]	0.25	3	—
E002	30	3.8	27 ± 3.0[a]	1.73[a]	0.25	5	—
FALL	28	3.7	27 ± 3.7	1.67 ± 0.07	0.22 ± 0.04	5	24.0 ± 4
WHIT	33	3.6	33 ± 3.2	1.74 ± 0.03	0.25 ± 0.01	0	31.5 ± 3
DEVL	30	3.8	14 ± 1.9[b]	1.88 ± 0.12[b]	0.30 ± 0.04	15	18.0 ± 4
FISH	25	3.7	14 ± 1.4[b]	1.83 ± 0.06[b]	0.30 ± 0.02	10	17.0 ± 4
MAGL	43	3.6	33 ± 4.7[a]	1.67 ± 0.04[a]	0.22 ± 0.02	3	—
SURP	30	3.6	27 ± 2.4	1.70 ± 0.02	0.24 ± 0.01	5	26.5 ± 2
Average	30 ± 5	3.7 ± 0.1	27 ± 6	1.75 ± 0.08	0.25 ± 0.03	5 ± 4	—
Transantarctic Mountains Interior (TAMI)							
LONW	40	3.7	37 ± 3.3[b]	1.87 ± 0.04[b]	0.30 ± 0.01	3	45.0 ± 5
MILR	40	3.7	36 ± 5.6[b]	1.79 ± 0.08[b]	0.27 ± 0.03	3	45.0 ± 10
DUFK	38	3.7	40 ± 3.9	1.76 ± 0.06	0.26 ± 0.03	0	38.4 ± 5
VNDA	35	3.8	35 ± 1.4[a]	1.78 ± 0.02[a]	0.27 ± 0.01	8	—
N000	38	3.6	39 ± 2.6[a]	1.70 ± 0.06[a]	0.24 ± 0.04	0	—
E004	35	3.8	34 ± 1.1[a]	1.76 ± 0.02[a]	0.26 ± 0.01	3	—
E006	35	3.7	30 ± 3.2[a]	1.70 ± 0.10[a]	0.24 ± 0.04	0	—
E008	38	3.7	38 ± 2.6[a]	1.75 ± 0.06[a]	0.26 ± 0.03	3	—
E010	40	3.7	39 ± 2.0[a]	1.77 ± 0.03[a]	0.27 ± 0.02	0	—
Average	38 ± 2	3.7 ± 0.1	36 ± 3	1.76 ± 0.05	0.26 ± 0.02	2 ± 2	—
Ellsworth Mountains (EWM)							
UNGL	38	3.7	37 ± 3.1[b]	1.78 ± 0.03[b]	0.27 ± 0.01	3	—
WILS	35	3.7	—	—	—	5	30.0 ± 5
HOWD	38	3.7	34 ± 3.0[b]	1.78 ± 0.04[b]	0.27 ± 0.02	3	37.0 ± 4
Average	37 ± 2	3.7	36 ± 2	1.78	0.27	4 ± 1	—
Marie Byrd Land (MBL)							
BEAR	33	3.8	24 ± 2.8	1.70 ± 0.08	0.24 ± 0.04	10	—
CLRK	30	3.6	30 ± 2.4	1.72 ± 0.02	0.24 ± 0.01	0	30.0 ± 2
MPAT	28	3.6	31 ± 2.5	1.65 ± 0.02	0.21 ± 0.01	0	27.5 ± 1
SILY	30	3.6	29 ± 2.4	1.90 ± 0.04	0.31 ± 0.01	3	32.8 ± 2
Average	30 ± 2	3.7 ± 0.1	29 ± 3	1.74 ± 0.11	0.25 ± 0.04	3 ± 5	—
Ross Island (RI)							
CBRI	25	3.6	19 ± 2.7[a]	1.88[a]	0.30	5	—
MINN	25	3.6	30 ± 2.4[a]	1.88[a]	0.30	3	—
Average	25	3.6	25 ± 6	1.88	0.30	4 ± 1	—
Other							
MECK	35	3.7	33 ± 2.8[b]	1.61 ± 0.04[b]	0.19 ± 0.03	8	26.5 ± 4
THUR	38	3.8	33 ± 4.6[b]	1.76 ± 0.12[b]	0.27 ± 0.06	5	24.1 ± 3

[a] *H–κ* parameters obtained from Finotello *et al.* (2011).
[b] *H–κ* parameters obtained from high-frequency receiver functions.

provided in Table 1 and Fig. 5 have been determined from Vp/Vs. The following sections describe the results based on individual tectonic regions.

4.1 Transantarctic Mountains front

For the TAMF region, the Moho depths found from the joint inversion method range from 23 to 43 km with an average of 30 ± 5 km. The crustal shear wave velocity ranges from 3.5 to 3.8 km s^{-1}, averaging 3.7 ± 0.1 km s^{-1}. The *H–κ* method gives Moho depths ranging from 14 to 33 km, with an average of 27 ± 6 km. Poisson's ratios for this region range from 0.20 to 0.30, with an average of 0.25 ± 0.03. The difference in the range of Moho depths between the two methods is mostly because of discrepant results for stations DEVL, FISH and MAGL (Table 1), which we address in the discussion section. The receiver functions for station TNV did not show a clear Ps arrival or other crustal multiples, potentially due to

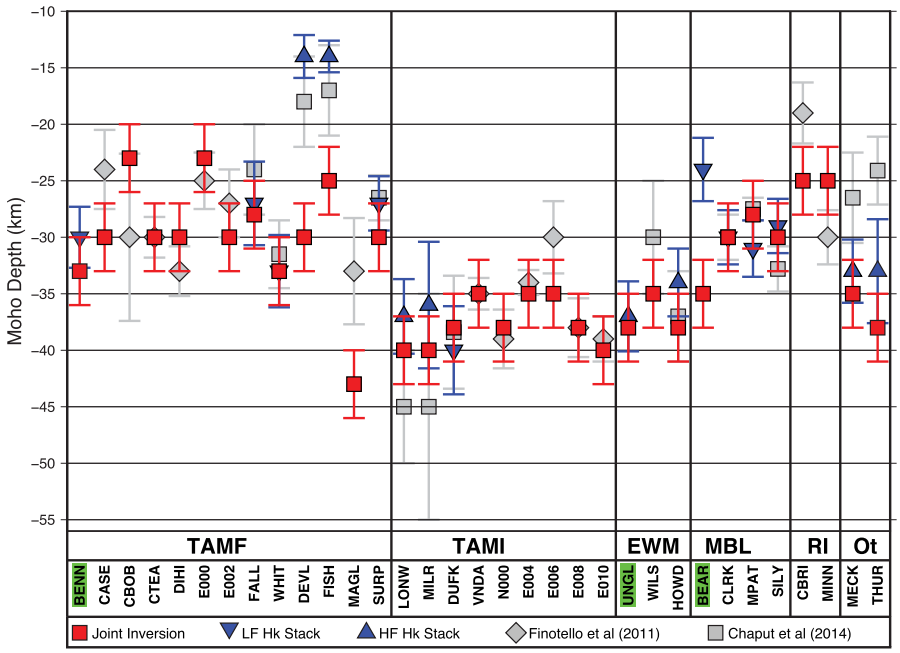

Figure 4. Moho depth results for the joint inversion and H–κ stacking. Red squares are results from the joint inversions. The blue triangles represent the H–κ stacking results. The grey diamonds are results from Finotello *et al.* (2011) and the grey squares are from Chaput *et al.* (2014). Stations with new results are highlighted in green. The different tectonic regions described in the text are labelled above station names.

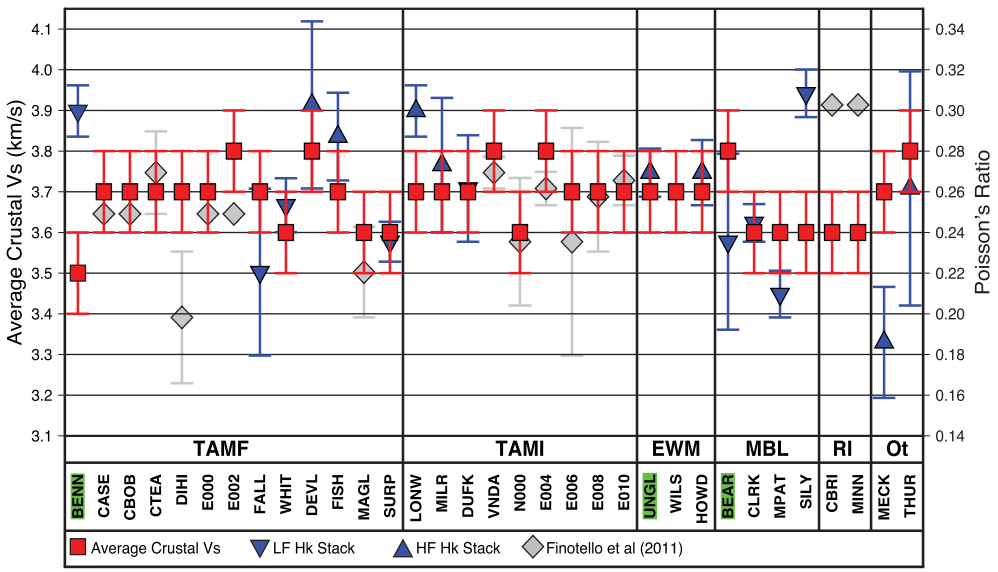

Figure 5. Average crustal S-wave velocity and Poisson's ratios. The red squares represent the average crustal Vs obtained from the joint inversion results. The blue triangles represent the Poisson's ratio calculated from the Vp/Vs ratios from the H–κ stacking. The grey diamonds represent Poisson's ratios from Finotello *et al.* (2011).

a gradational Moho, and therefore we do not report results for this station.

4.2 Transantarctic Mountains internal

Crustal thicknesses in the TAMI region range from 35 to 40 km, with an average of 38 ± 2 km. The crustal velocity for all the stations ranges from 3.6 to 3.8 km s^{-1}, averaging 3.7 ± 0.1 km s^{-1}. H–κ stacking yielded an average Moho depth of 36 ± 3 km, with a range of 30 to 40 km. The Poisson's ratio for this region is 0.26 ± 0.2. Similar to station TNV, we did not obtain results from the joint inversion or H–κ stacking methods for station PECA.

4.3 Ellsworth Mountains

The Moho depths from the joint inversion technique in the EWM block range from 35 to 38 km with an average of 37 ± 2 km. The crustal shear wave velocity is 3.7 km s^{-1} for all of the stations. The results from the H–κ method show 34 and 37 km thick crust for stations HOWD and UNGL, respectively. A Poisson's ratio of 0.27 was obtained for both of those stations. WILS has a Moho Ps arrival

that is clear on the receiver functions, and we were able to obtain a result for the joint inversion, but an H–κ stacking result was not obtained because other crustal multiples were not clearly observed.

4.4 Marie Byrd Land

Moho depths for the MBL stations from the joint inversion range from 28 to 33 km, with an average of 30 ± 2 km. BEAR station has an average shear wave velocity of 3.8 km s^{-1}, whereas the other three stations in this block have an average of 3.6 km s^{-1}. Moho depths from the H–κ stacking range from 24 to 31 km, averaging 28 ± 3 km. Poisson's ratios for the stations average to 0.25 ± 0.04.

4.5 Ross Island

Crustal thickness estimations using the joint inversion method for both stations in this region yielded 25 km. Crustal shear wave velocities for all stations are 3.6 km s^{-1}. The Moho depths from the H–κ stacking range from 19 to 30 km, with an average of 25 ± 6 km. The average Poisson's ratio for the stations in this region is 0.30. There were insufficient high-quality receiver functions for stations SBA and CCRZ to obtain results.

5 DISCUSSION

In this section we compare our results to previous results and comment on the composition of the crust and the origin of several of the tectonic blocks. We also emphasize results from three stations for which no previous estimates of crustal structure have been reported. Station BENN in the TAMF region has a crustal thickness of 33 km, average crustal Vs of 3.5 km s^{-1}, and a Poisson's ratio is 0.30. For station UNGL in the EWM region, the Moho depth is 38 km, the average crustal Vs is 3.7 km s^{-1}, and the Poisson's ratio is 0.27. Station BEAR, on the margin of MBL, has a crustal thickness of 33 km, average crustal Vs of 3.8 km s^{-1}, and Poisson's ratio of 0.24.

Stations MECK and THUR are in different tectonic regions and so we discuss them individually. Station MECK has a low Poisson's ratio (0.19) along with intermediate crustal Vs (3.7 km s^{-1}) suggesting a felsic composition. THUR has an intermediate crustal composition indicated by the Poisson's ratio of 0.27 and average crustal Vs of 3.8 km s^{-1}.

5.1 Moho interpretation

Although the Moho can be identified in the velocity profiles for most of the stations as a velocity discontinuity where Vs increases to ≥4.3 km s^{-1}, as discussed previously, for all stations shown in Fig. 6, identifying the Moho is not necessarily straightforward. For these stations, the velocity profiles show a significant velocity discontinuity at a depth shallower than our preferred Moho pick where Vs increases to ≥4.3 km s^{-1} (Fig. 6). Layers between these two depths have velocities of ∼4.0–4.2 km s^{-1}, for which there are several possible interpretations. One interpretation is that this is thermally perturbed upper mantle. However, this interpretation would require a temperature anomaly of >100 °C, given that velocities at these stations below ∼50 km depth range from 4.3 to 4.5 km s^{-1}. Another possibility is that the rocks at these depths are compositionally distinct upper-mantle rocks. Mantle lithologies are not always homogenous, and Lizarralde *et al.* (2004) have suggested that there could be gabbroic compositions retained in the mantle, which would reduce mantle velocities. Yet another possible explanation is seismic anisotropy. Seismic velocities can vary by 3.5–4.5 per cent or 0.15–0.20 km s^{-1} depending on direction as measured from xenoliths at depths of 40–170 km (Savage 1999). However, given the localized nature of the observations at just a few isolated stations, it is difficult to attribute the layers with 4.0–4.2 km s^{-1} velocities to either mantle composition or anisotropy. Our preferred interpretation is that the 4.0–4.2 km s^{-1} velocities represent mafic rocks in the lower crust, which are commonly found in many continental settings (e.g. Rudnick & Gao 2003; Kachingwe *et al.* 2015).

5.2 Comparison with previous studies

A comparison between previous work and our results shows consistency within the reported uncertainties (Table 1, Fig. 4) for all but four stations. At stations DEVL, FISH, MECK and THUR, our joint inversion results do not match with previous results from Chaput *et al.* (2014). For these stations, Moho depths obtained from the joint inversion method are substantially greater than those reported in Chaput *et al.* (2014). For stations DEVL, FISH, MAGL, CBRI and BEAR, the joint inversion result is also not consistent with the H–κ result (Table 1, Fig. 6a). As previously mentioned, the Moho depth in the joint inversion method is selected where shear wave velocities exceed 4.3 km s^{-1}. At these stations, there are a few layers above the Moho with velocities of 4.0–4.2 km s^{-1} Therefore, the shallower 'Moho' depths obtained from the H–κ stacking and/or reported by Chaput *et al.* (2014) are interpreted to be mid-crustal discontinuities, with ∼10–20 km of mafic lower crust separating the mid-crustal discontinuity from the Moho.

For stations that are in close proximity, our estimates of crustal thickness are also similar to those reported by Bannister *et al.* (2003). Both studies utilize station VNDA and report crustal thickness of 35 km. Station E000 yielded a crustal thickness of 23 km and is located station AN05 in the Bannister *et al.* (2003) study, which has a crustal thickness of 18 km. Stations E002 and E004 have crustal thicknesses of 32 and 35 km respectively, which is similar to the 32 km crustal thickness reported for station AN10. E008 and E010 have crustal thicknesses of 38 and 40 km, similar to the 40 km thick crust found at station AN08.

5.3 Crustal composition

With a complete suite of shear wave velocity profiles and estimates of Poisson's ratio for each station, the composition of the crust in each tectonic region can be investigated. As described above, shear wave velocities greater than 3.9 km s^{-1} indicate the presence of mafic rocks. Following Christensen (1996) and Tarkov & Vavakin (1982), we take Poisson's ratios of 0.20–0.24 to indicate a bulk felsic composition for the crust, ratios of 0.25–0.27 to indicate a felsic to intermediate composition, and ratios of 0.28–0.30 to indicate a mafic composition.

5.3.1 Transantarctic Mountain front

The bulk crustal composition in this region is felsic to intermediate but stations BENN, DEVL and FISH have Poisson's ratio that suggest an intermediate to mafic crustal composition. However, the average crustal Vs for station BENN is only 3.5 km s^{-1}, which is not consistent with a mafic crust. The joint inversion results show a 2.5 km thick low velocity layer at the surface, indicating sediments beneath the station. The sediments, particularly if they are

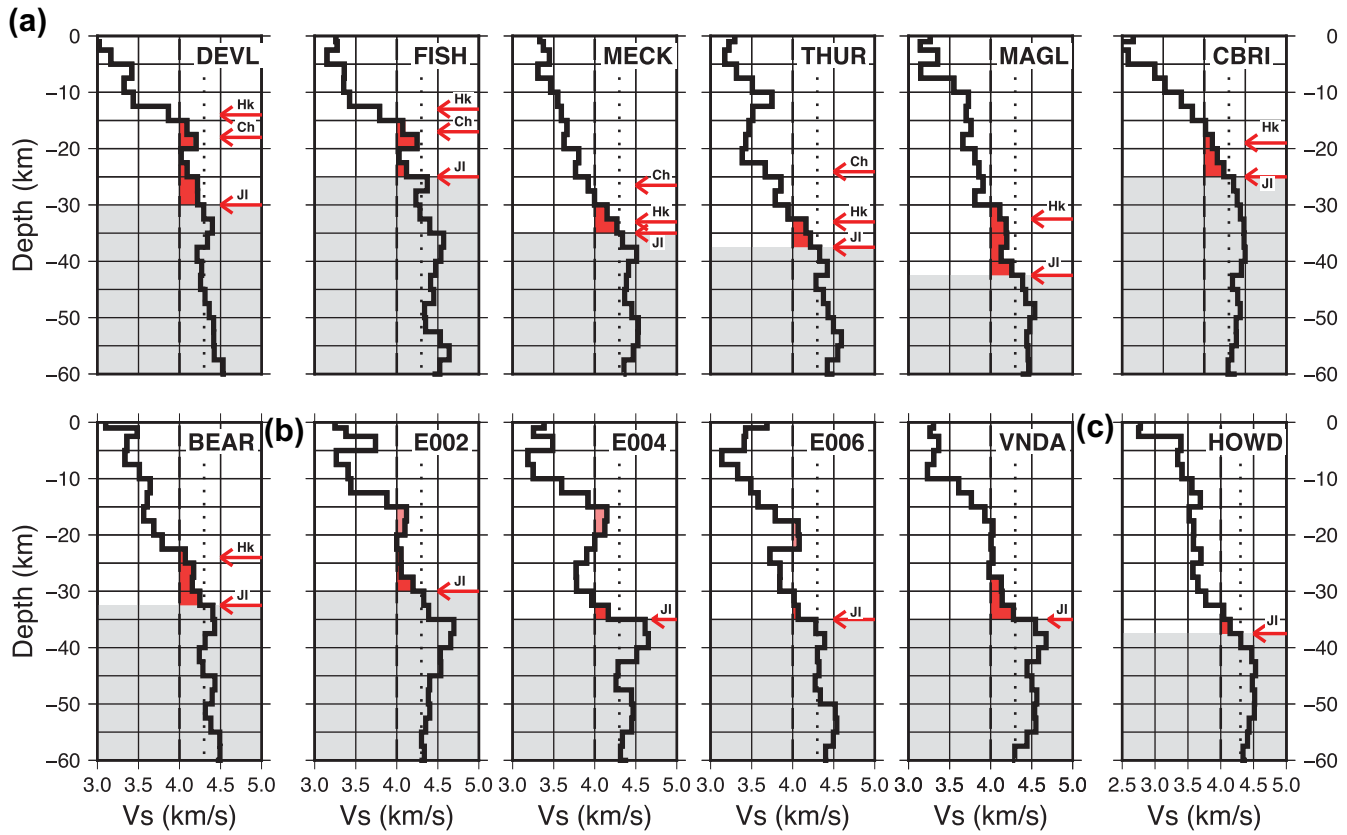

Figure 6. Shear wave velocity profiles for selected stations discussed in the text. The red arrows represent Moho depths for the following: JI, Joint inversion; Hk, *H*–κ stacking; Ch, Chaput *et al.* (2014). Grey fill in the figures represents mantle depths. Red colour shows the regions we have interpret as a mafic lower crust. (a) Stations where Moho depths derived from joint inversion are different from that of the *H*–κ method and/or those obtained from Chaput *et al.* (2014). The different interpretations are explained in the text. (b) Shear wave velocity profiles for stations in the TAM. The mid crustal mafic layering is most prominent in stations E004 and E006 in the TAM between ∼15 and ∼25 km depth and stations E002 and VNDA below 15 km. (c) Shear wave velocity profile for station HOWD.

unconsolidated, could be influencing the average crustal Poisson's ratio.

The thickness of mafic layers in the lower crust range from 0 to 5 km for all the stations in this region except for stations DEVL, E002, FISH and MAGL, where the mafic lower crust is 10 to 15 km thick. Since these stations are located within a region of mapped Ferrar basaltic flows and intrusions (Elliot *et al.* 1999), a possible explanation for the thick mafic lower crust at these stations is the addition of mafic material to the lower crust during the Ferrar magmatic event.

5.3.2 *Transantarctic Mountains internal*

The average crustal Vs (3.7 km s^{-1} ± 0.1 km s^{-1}) and the average Poisson's ratio (0.26 ± 0.02) for this region suggest an overall bulk crustal composition that is felsic to intermediate. The only station that could be interpreted to have a more mafic composition is LONW, which has a Poisson's ratio of 0.30. There is a wide range in crustal thicknesses in this region, and this is most likely related to crustal thinning near the mountain front. Fig. 7 shows a clear relationship between the crustal thickness and station distance from the coast, with about a 10 km change in crustal thickness between the TAM front and the TAM interior.

Several stations in this block have high velocities (Vs ≥ 4.0 km s^{-1}) within the crust. Station E004 has a thin mafic lower crust of 3 km, but a 10–13 km thick layer with a Vs of ∼4.0 km s^{-1} in the mid crust (Fig. 6). This mid-crustal high velocity layer is also observed at stations E006 and E002 in the TAM (Fig. 6). At station VNDA, the bottom ∼18 km of the crust has high velocities between 4.0 km s^{-1} and 4.3 km s^{-1} (Fig. 6).

The Ferrar Dolerites, which define a magmatic province covering a large portion of the TAM, intruded into the Beacon Supergroup around ∼176 Ma (Flemming *et al.* 1997). It has been suggested that the confinement of dolerite exposures in linear features within the TAM was a result of pre-existing zones of weakness within the lithosphere (Fitzgerald *et al.* 1986). Although the geochemistry is mostly uniform across the Ferrar Province, the magmatic feeder system could have been sourced from distinct locations in the mantle that were connected at greater depths (Encarnacion *et al.* 1996). The absence of a crustal root system for the magmatism could account for the localized crustal modification we observe at stations DEVL, E002, FISH and MAGL in the TAMF region and stations E004, E006 and VNDA in the TAMI region, but not pervasively throughout the TAM.

5.3.3 *Ellsworth Mountains*

The bulk crustal composition of the EWM is intermediate as indicated by an average Poisson's ratio of 0.27. Overall, the crustal structure of the EWM is similar to that of the TAMI, with

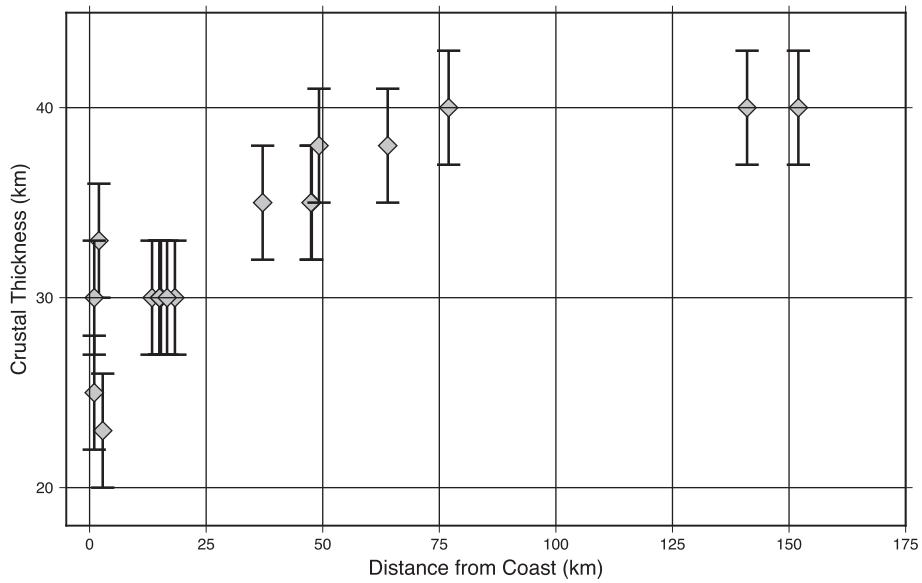

Figure 7. Joint inversion crustal thickness versus distance from the coast for stations in the TAM.

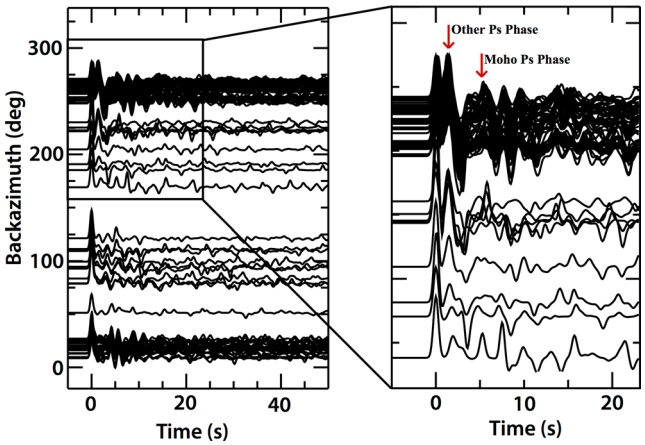

Figure 8. High-frequency receiver functions for station HOWD. Receiver functions from the 210–270 backazimuth range have a phase arriving between 1 and 2 s, interpreted as a Ps conversion from the base of a sedimentary basin near the station.

comparable crustal thicknesses and Poisson's ratios. There is also a lack of a thick mafic lower crust in the EWM region. The similarity in crustal structure with the TAM strengthens the hypothesis that the EWM is a rotated block from the TAM (Webers *et al.* 1992; Dalziel *et al.* 2013).

The receiver functions for station HOWD indicate azimuthal variation in upper crustal structure (Fig. 8). On the high-frequency receiver functions, a Ps phase is observed arriving at roughly 1.5 s but only from backazimuths of 210°–270°, while the Moho Ps arrives at around 5 s from all backazimuths. For this particular station, we performed two separate inversions, one using all of the data and another with only receiver functions with 210°–270° backazimuth. The joint inversion for the limited dataset shows a low velocity layer at the surface. We interpret this layer as an indication of sediments located within a basin next to the station. The shear wave velocity profile obtained has a 2.5 km low velocity layer at the surface and a Moho at a 38 km depth (Fig. 6). The same crustal thickness is obtained from both datasets, suggesting that the azimuthal variation is restricted to the upper few kilometres of the crust.

5.3.4 Marie Byrd Land

The four stations in MBL reveal a range of crustal structure in this tectonic block. Stations CLRK and MPAT have similar crustal thickness of 30 and 28 km, and crustal composition that is felsic to intermediate, as indicated by an average crustal Vs of 3.6 km s^{-1} and Poisson's ratios of 0.24 and 0.21. Although station SILY has a crustal thickness of 30 km and average crustal Vs of 3.6 km s^{-1}, the Poisson's ratio for this station is 0.31. This high Poisson's ratio suggests a mafic composition, whereas the average crustal Vs of 3.6 km s^{-1} suggests an intermediate composition. This apparent contradiction can be resolved by the presence of partial melt underneath the station, which would reduce average shear wave velocity, increasing the Vp/Vs and Poisson's ratio as well reducing the average crustal Vs. An active zone of deep crustal/uppermost mantle seismicity has been detected near SILY (Lough *et al.* 2013), which supports the presence of partial melt and mobile magma or magmatically linked fluids in the lower crust beneath this station. Alternatively, the crust could be comprised of a significant amount of volcaniclastic material, which also leads to a reduction in the mean crustal Vs.

At station BEAR, the crust has a crustal thickness of 33 km, an average Vs 3.8 km s^{-1} and a Poisson's ratio of 0.24. The Poisson's ratio is relatively low for a crustal composition that is suggested by a crustal Vs of 3.8 km s^{-1}. As noted previously, the H–κ method gave a depth to a mid-crustal discontinuity and therefore the Vp/Vs obtained is only representative of the upper crust and not the entire crust (Fig. 6). The 10 km thick mafic lower crust that we observe at this station may be a result of coeval magmatic modification of the lower crust with the widespread Cenozoic volcanic activity within MBL (LeMasurier & Rex 1989).

5.3.5 Ross Island

The Cenozoic volcanic rocks that are found on and surrounding Ross Island are mostly tephrites and basinites (Kyle *et al.* 1992). Stations CBRI and MINN have a high Poisson's ratio of 0.30, consistent with a mafic crust. However, the average crustal Vs of 3.6 km s^{-1} for these stations suggests an intermediate crustal composition. This apparent discrepancy can be attributed to either a

significant amount of volcaniclastic material comprising the crust, which would lower the Vs compared to intrusive mafic rocks, or the presence of partial melt in the crust. The thin crust (25 km) can be explained by Cenozoic rifting associated with the Terror Rift, which terminates at the northern end of the Ross Island, and the initiation of this localized rifting is thought to be coeval with the onset of volcanism (Kyle *et al.* 1992; Trey *et al.* 1999).

6 SUMMARY

We use a joint inversion technique and the H–κ stacking method to obtain a uniform suite of crustal structure parameters that allow us to compare the nature of the crust between different tectonic blocks. New results on crustal structure are reported for three stations (BEAR, BENN and UNGL). On average, the TAMF region has a thinner crust and slightly lower Poisson's ratio than the interior of the TAM. We also find some evidence in the TAM for crustal modification possibly related to the Ferrar magmatic event. However, locations where magmatic modification of the crust occurs suggest that modification is not a pervasive feature in the TAM. The crust of the EWM is similar to that of the TAM, supporting the origin of the EWM as a rotated block from the TAM. In MBL, the crustal parameters show a range of composition, including possible evidence for partial melt under station SILY. And finally, the RI region has a high Poisson's ratio, thin crust and intermediate average crustal Vs, all consistent the Cenozoic volcanism found there and the proximity of the region to the Terror Rift.

ACKNOWLEDGEMENTS

We thank the National Science Foundation (NSF) Office of Polar Programs (grants 1249631, 1249602, 1249513, 1246666, 1246712, 1246776, 1247518, 0632230, 0632239, 0652322, 0632335, 0632136, 0632209) and 0632185 for their support of the Polar Earth Observing Network - Antarctica Network (POLENET-ANET) project. The seismic deployments in this study benefited greatly from the technical support of the Incorporated Research Institutions for Seismology (IRIS) through the Portable Array Seismic Studies of the Continental Lithosphere (PASSCAL) Instrument Center at New Mexico Tech. Seismic data are freely available at the IRIS Data Management Center. The facilities of the IRIS Consortium are supported by the National Science Foundation under Cooperative agreement EAR-1063471. Thanks to Patrick Shore for providing invaluable support in collecting and archiving data from all the projects used. Some figures were made using the freely available software 'Generic Mapping Tools' (GMT). We also would like to thank two anonymous reviewers for greatly improving this paper with their comments.

REFERENCES

Accardo, N.J. *et al.*, 2014. Upper mantle seismic anisotropy beneath the west Antarctic rift system and surrounding region from shear wave splitting analysis, *Geophys. J. Int.,* **198,** 414–429.

Anthony, R., Aster, R., Wiens, D., Nyblade, A., Anandakrishnan, S., Winberry, J.P., Wilson, T. & Rowe, C., 2014. The seismic noise environment of Antarctica, *Seismol. Res. Lett.,* **86,** 89–100.

Bannister, S., Yu, J., Leitner, B. & Kennett, B.L.N., 2003. Variations in crustal structure across the transition from West to East Antarctica, Southern Victoria Land, *Geophys. J. Int.,* **155,** 870–884.

Cassidy, J., 1992. Numerical experiments in broadband receiver function analysis, *Bull. seism. Soc. Am.,* **82,** 1453–1474.

Chaput, J. *et al.*, 2014. The crustal thickness of West Antarctica, *J. geophys. Res.,* **119,** 378–395.

Christensen, N.I., 1996. Poisson's ratio and crustal seismology, *J. geophys. Res.,* **101,** 3139–3156.

Christensen, N.I. & Mooney, W.D., 1995. Seismic velocity structure and composition of the continental crust: a global view, *J. geophys. Res.,* **100,** 9761–9788.

Dalziel, I.W.D., Lawver, L.A., Norton, I.O. & Gahagan, L.M., 2013. The scotia Arc: genesis, evolution, global significance, *Annu. Rev. Earth Planet. Sci.,* **41,** 767–793.

Dziewonski, A.M. & Anderson, D.L., 1981. Preliminary reference Earth model, *Phys. Earth planet. Inter.,* **25,** 297–356.

Elliot, D.H., Fleming, T.H., Kyle, P.R. & Foland, K.A., 1999. Long-distance transport of magmas in the Jurassic Ferrar Large Igneous Province, Antarctica, *Earth planet. Sci. Lett.,* **167,** 89–104.

Efron, B. & Tibshirani, R., 1991. Statistical data analysis in the computer age, *Science,* **253**(5018), 390–395.

Emry, E.L., Nyblade, A.A., Julià, J., Anandakrishnan, S., Aster, R.C., Wiens, D.A., Huerta, A.D. & Wilson, T.J., 2015. The mantle transition zone beneath West Antarctica: seismic evidence for hydration and thermal upwellings, *Geochem. Geophys. Geosyst.,* **16,** 40–58.

Encarnación, J., Fleming, T.H., Elliot, D.H. & Eales, H.V., 1996. Synchronous emplacement of Ferrar and Karoo dolerites and the early breakup of Gondwana, *Geology,* **24,** 535–538.

Finotello, M., Nyblade, A., Julia, J., Wiens, D. & Anandakrishnan, S., 2011. Crustal Vp–Vs ratios and thickness for Ross Island and the Transantarctic Mountain front, Antarctica, *Geophys. J. Int.,* **185,** 85–92.

Fitzgerald, P.G., 1992. The transantarctic Mountains of southern Victoria Land: the application of apatite fission track analysis to a rift shoulder uplift, *Tectonophysics,* **11,** 634–662.

Fitzgerald, P.G., Sandiford, M., Barrett, P.J. & Gleadow, A.J.W., 1986. Asymmetric extension associated with uplift and subsidence in the Transantarctic Mountains and Ross Embayment, *Earth planet. Sci. Lett.,* **81,** 67–78.

Flemming, T.H., Heimann, A., Foland, K.A. & Elliot, D.H., 1997. $^{40}Ar/^{39}Ar$ geochronology of Ferrar Dolerite sills from the Transantarctic Mountains, Antarctica: implications for the age and origin of the Ferrar magmatic province, *Bull. geol. Soc. Am.,* **109,** 533–546.

Fretwell, P. *et al.*, 2013. Bedmap2: improved ice bed, surface and thickness datasets for Antarctica, *Cryosphere,* **7,** 375–393.

Graw, J.H., Adams, A.N., Hansen, S.E., Wiens, D.A., Hackworth, L. & Park, Y., 2016. Upper mantle shear wave velocity structure beneath northern Victoria Land, Antarctica: volcanism and uplift in the northern Transantarctic Mountains, *Earth planet. Sci. Lett.,* **449,** 48–60.

Hall, J., Wilson, T. & Henrys, S., 2007. Structure of the central terror rift, Western Ross Sea, Antarctica, 1–5, doi:10.3133/of2007-1047.srp108.

Hansen, S.E., Nyblade, A.A., Heeszel, D.S., Wiens, D.A., Shore, P. & Kanao, M., 2010. Crustal structure of the Gamburtsev Mountains, East Antarctica, from S-wave receiver functions and Rayleigh wave phase velocities, *Earth planet. Sci. Lett.,* **300**(3), 395–401.

Hansen, S.E. *et al.*, 2014. Imaging the Antarctic mantle using adaptively parameterized *P*-wave tomography: evidence for heterogeneous structure beneath West Antarctica, *Earth planet. Sci. Lett.,* **408,** 66–78.

Heeszel, D.S. *et al.*, 2016. Upper mantle structure of central and West Antarctica from array analysis of Rayleigh wave phase velocities, *J. geophys. Res.,* **121,** 1758–1775.

Holbrook, W.S., Mooney, W.D. & Christensen, N.I., 1992. The seismic velocity structure of the deep continental crust, in *Continental Lower Crust,* Chap. 1, pp. 1–43, eds Fountain, D.M., Arculus, R. & Kay, R.W., Elsevier.

Julià, J., 2007. Constraining velocity and density contrasts across the crust–mantle boundary with receiver function amplitudes, *Geophys. J. Int.,* **171,** 286–301.

Julia, J., Ammon, C.J., Herrmann, R.B. & Correig, A.M., 2000. Joint inversion of receiver function and surface wave dispersion observations, *Geophys. J. Int.,* **143,** 99–112.

Julià, J., Ammon, C.J. & Herrmann, R.B., 2003. Lithospheric structure of the Arabian Shield from the joint inversion of receiver functions and surface-wave group velocities, *Tectonophysics,* **371,** 1–21.

Julià, J., Ammon, C.J. & Nyblade, A.A., 2005. Evidence for mafic lower crust in Tanzania, East Africa, from joint inversion of receiver functions and Rayleigh wave dispersion velocities, *Geophys. J. Int.,* **162,** 555–569.

Kachingwe, M., Nyblade, A. & Julià, J., 2015. Crustal structure of Precambrian terranes in the southern African subcontinent with implications for secular variation in crustal genesis, *Geophys. J. Int.,* **202**(1), 533–547.

Kyle, P.R., 1990. McMurdo Volcanic Group, western Ross Embayment: introduction, in *Antarctic Research Series American Geophysical Union,* vol. 48, pp. 19–25, eds LeMasurier, W.E. & Thomson, J.W., Volcanoes of the Antarctic Plate and Southern Oceans.

Kyle, P.R., Moore, J.A. & Thirlwall, M.F., 1992. Petrologic evolution of anorthoclase phonolite lavas at Mount Erebus, Ross Island, Antarctica, *J. Petrol.,* **33,** 849–875.

Langston, C.A., 1979. Structure under Mount Rainier, Washington, inferred from teleseismic body waves, *J. geophys. Res.,* **84,** 4749–4762.

Lawrence, J.F., Wiens, D.A., Nyblade, A.A., Anandakrishnan, S., Shore, P.J. & Voigt, D., 2006a. Upper mantle thermal variations beneath the Transantarctic Mountains inferred from teleseismic *S*-wave attenuation, *Geophys. Res. Lett.,* **33,** 2–5.

Lawrence, J.F., Wiens, D.A., Nyblade, A.A., Anandakrishnan, S., Shore, P.J. & Voigt, D., 2006b. Rayleigh wave phase velocity analysis of the Ross Sea, Transantarctic Mountains, and East Antarctica from a temporary seismograph array, *J. geophys. Res.,* **111,** 1–15.

Lawrence, J.F., Wiens, D.A., Nyblade, A.A., Anandakrishnan, S., Shore, P.J. & Voigt, D., 2006c. Crust and upper mantle structure of the transantarctic mountains and surrounding regions from receiver functions, surface waves, and gravity: implications for uplift models, *Geochem. Geophys. Geosyst.,* **7,** doi:10.1029/2006GC001282.

LeMasurier, W.E. & Rex, D.C., 1989. Evolution of linear volcanic ranges in Marie Byrd Land, West Antarctica, *J. geophys. Res.,* **94,** 7223–7236.

Ligorría, J.P. & Ammon, C.J., 1999. Iterative deconvolution and receiver-function estimation, *Bull. seism. Soc. Am.,* **89,** 1395–1400.

Lizarralde, D., Gaherty, J., Collins, J., Hirth, G. & Kim, S., 2004. Spreading-rate dependence of melt extraction at mid-ocean ridges from mantle seismic refraction data, *Nature,* **432,** 744–747.

Lloyd, A.J., Wiens, D.A., Nyblade, A.A. & Anandakrishnan, S., 2015. A seismic transect across West Antarctica: evidence for mantle thermal anomalies beneath the Bentley Subglacial Trench and the Marie Byrd Land Dome, *J. geophys. Res.,* **120,** 8439–8460.

Lough, A.C. *et al.*, 2013. Seismic detection of an active subglacial magmatic complex in Marie Byrd Land, Antarctica, *Nat. Geosci.,* **6,** 1031–1035.

Owens, T.J. & Zandt, G., 1985. The response of the continental crust- mantle boundary observed on broadband teleseismic receiver functions, *Geophys. Res. Lett.,* **12,** 705–708.

Pondrelli, S., Amato, A., Chiappini, M., Cimini, G.B., Colombo, D. & Di Bona, M., 1997. ACRUP1 Geotraverse: contribution of teleseismic data recorded on land, in *The Antarctic Region: Geological Evolution and Processes*, pp. 631–635, ed. Ricci, C.A., Terra Antartica Publication.

Ramirez, C. *et al.*, 2016. Crustal and upper-mantle structure beneath ice-covered regions in Antarctica from *S*-wave receiver functions and implications for heat flow, *Geophys. J. Int.,* **204,** 1636–1648.

Rudnick, R.L. & Fountain, D.M., 1995. Nature and composition of the continental crust: A lower crustal perspective, *Rev. Geophys.,* **33,** 267–309.

Rudnick, R.L. & Gao, S., 2003. Composition of the continental crust, in *Treatise on Geochemistry,* Vol. 3, pp. 1–64, ed. Rudnick, R.L., Elsevier.

Savage, M.K., 1999. Seismic anisotropy and mantle deformation: what have we learned from shear wave splitting?, *Rev. Geophys.,* **37,** 65–106.

Sun, X., Wiens, D.A., Nyblade, A., Anandakrishnan, S., Aster, R.C., Chaput, J.A., Huerta, A.D. & Wilson, T.J., 2013. Three-dimensional crust and upper mantle velocity structure of Antarctica from seismic noise correlation, in *AGU Fall Meeting Abstracts*, vol. 1, pp. 2.

Tarkov, A.P. & Vavakin, V.V., 1982. Poisson's ratio behaviour in various crystalline rocks: application to the study of the Earth's interior, *Phys. Earth planet. Inter.,* **29,** 24–29.

Ten Brink, U.S., Hackney, R.I., Bannister, S., Stern, T.A. & Makovsky, Y., 1997. Uplift of the Transantarctic Mountains and the bedrock beneath the East Antarctic ice sheet, *J. geophys. Res.,* **102,** 27 603–27 621.

Trey, H., Cooper, A.K., Pellis, G., Della Vedova, B., Cochrane, G., Brancolini, G. & Makris, J., 1999. Transect across the West Antarctic rift system in the Ross Sea, Antarctica, *Tectonophysics,* **301,** 61–74.

Watson, T., Nyblade, A., Wiens, D.A., Anandakrishnan, S., Benoit, M., Shore, P.J., Voigt, D. & VanDecar, J., 2006. *P* and *S* velocity structure of the upper mantle beneath the Transantarctic Mountains, East Antarctic craton, and Ross Sea from travel time tomography, *Geochem. Geophys. Geosyst.,* **7,** doi:10.1029/2005GC001238.

Webers, G.F., Craddock, C. & Splettstoesser, J.F., 1992. Geologic history of the Ellsworth Mountains, West Antarctica, *Mem. - Geol. Soc. Am.,* **170,** 1–8.

Yoshida, M., 1982. Superposed deformation and its implication to the geologic history of the Ellsworth Mountains, West Antarctica, *Mem. Natl. Inst. Polar Res. Spec. Issue,* **21,** 120–171.

Zandt, G. & Ammon, C.J., 1995. Continental crust composition constrained by measurements of crustal Poisson's ratio, *Nature*, **374,** 152–154.

Zhu, L. & Kanamori, H., 2000. Moho depth variation in southern California from teleseismic receiver functions, *J. geophys. Res.,* **105,** 2969–2980.

SUPPORTING INFORMATION

Supplementary data are available at *GJI* online.

Appendix A: H–κ stacking results for the stations.
Appendix B: Joint inversion results for all of the stations.
Appendix C: Individual receiver.

Please note: Oxford University Press is not responsible for the content or functionality of any supporting materials supplied by the authors. Any queries (other than missing material) should be directed to the corresponding author for the paper.